



Dynamic tuning of naked ruthenium clusters/nanoparticles in ionic liquids cages to boost CO₂ hydrogenation to formic acid

Muhammad I. Qadir ^{a,1,*}, Marcus V. Castegnaro ^b, Felipe F. Selau ^b, Daniel L. Baptista ^b, Gustavo Chacon ^c, Renato B. Pontes ^d, Allan M. Lisbôa ^e, Dario Eberhardt ^e, Jairton Dupont ^{c,f,2,**}

^a Instituto de Química-Universidade Federal de Goiás-UFG, Av. Esperança s/n, Campus Samambaia, 74690-900 Goiânia, Goiás, Brazil

^b Instituto de Física, Universidade Federal do Rio Grande do Sul (UFRGS), Av. Bento Gonçalves, 9500, Porto Alegre 91501-970, RS, Brazil

^c Institute of Chemistry-UFRGS, Av. Bento Gonçalves, 9500, Porto Alegre 91501-970, RS, Brazil

^d Instituto de Física, Universidade Federal de Goiás-UFG, Av. Esperança s/n, Campus Samambaia, 74690-900 Goiânia, Goiás, Brazil

^e PUCRS, Centro Interdisciplinar de Nanociencias e Micro-Nanotecnologia, Porto Alegre 90619-900, RS, Brazil

^f Departamento de Biología Molecular B e Inmunología Facultad de Química, Universidad de Murcia, P.O. Box 4021, E-30100 Murcia, Spain

ARTICLE INFO

Keywords:

Ruthenium clusters
Carbon dioxide
Selective hydrogenation
Ionic liquids cages
SILPs

ABSTRACT

The reduction of atmospheric CO₂ is indeed a major challenge for modern life due to its increase as a result of the intensified contemporary industrial activities and its contribution to global warming. One of the most desirable approaches to accomplish this goal is to convert CO₂ into C1 feedstocks, such as formic acid (FA). In this regard, naked ruthenium clusters and nanoparticles (1.8 ± 0.3 nm) are prepared by magnetron sputtering into different supported ionic liquid phases (SILPs) that demonstrated remarkable efficiency in producing a total of 2.2 M of free FA with a TONs of 7305 in 1-Butyl-3-methylimidazolium acetate ionic liquid media at 87 °C. The higher efficiency is related to the hydrophobic/hydrophilic effect present in the ionic liquid-cages of the SILPs akin to the micelle nano (micro)reactors, which act as catalytic membranes enabling the tuning of FA production. DFT calculations support the mechanistic approach followed the hydrogenation of HCO₃[–] to FA.

1. Introduction

Emissions of carbon dioxide have received worldwide attention because of the environmental and economic threats posed by climate change [1,2]. The reduction of CO₂ as well as its conversion to value added chemicals and fuels is the main challenge facing research community. Although pure CO₂ can be obtained from the atmosphere by the CO₂ capture technologies such as absorption, adsorption, cryogenics, and membrane separation [3,4]. But its transportation and storage process is at economic and energy cost [5]. One of the best ways is to utilize and convert it (catalytically) into the sustainable valuable commodities such as formic acid (FA), methanol, higher hydrocarbons, carbonates (cyclic), formaldehyde, dimethyl ether and carbon monoxide thermally and photochemically [5–11]. Among them, by coupling the hydrogen and CO₂ into FA addresses to realize a hydrogen-based economy. FA is attractive hydrogen carrier with the volumetric H₂

density of 53 g of H₂/litre [12].

Capturing and activating CO₂ with ionic liquids (ILs) is a highly promising approach among the various emerging technologies aimed for dealing with the increasing CO₂ emissions [13,14]. The unique properties of ILs offer advantages during the hydrogenation of CO₂, as evidenced by the recent activity in this area [15–21]. ILs specially the imidazolium ones can generate the solvent “cage” around the catalysts (NPs, complexes and enzyme) akin to the micelle nano (micro)reactors, that can selectively control the diffusion of reactants, intermediates, and products, mainly through their hydrophobicity and contact ion pairs to the catalytically active sites [22–27]. This cage effect was revealed several times in reactions performed in both bare ILs and hybrids containing ILs [25,28]. However, there is still a lack of understanding regarding the correlation between the IL-catalyst structure and performance during CO₂ reduction. In the clear majority of the cases the CO₂ hydrogenation is performed by homogenous based catalysts (Ru, Rh and

* Corresponding author.

** Corresponding author at: Institute of Chemistry-UFRGS, Av. Bento Gonçalves, 9500, Porto Alegre, 91501-970 RS, Brazil.

E-mail addresses: irfan@ufg.br (M.I. Qadir), jairton.dupont@ufrgs.br (J. Dupont).

¹ ORCID: 0000-0001-7172-8427.

² ORCID: 0000-0003-3237-0770.



Ir) in the presence of the bases producing formates but not free formic acid. Amines functionalized ILs with ruthenium complexes have been studied that hydrogenate CO_2 exclusively to formate salts (not FA) [29–31]. Recently, homogeneous system based on Ru-complexes with sophisticated ligands have been reported to generate FA in BMIm.OAc IL system and represented activity from few thousands to several thousand TONs ($1950-8 \times 10^5$) [16,32–34]. Only in a few cases the hydrogenation of CO_2 has been performed by heterogeneous catalysts under severe reaction conditions (40 MPa) but generally with low catalytic performance [35–37]. CO_2 hydrogenation to free FA by well-defined metal nanoparticles is rare.

Moreover, the contribution of buffer-like solutions versus the Ru clusters/NPs during CO_2 hydrogenation is usually overlooked and not fully explored. It is usually assumed that the interaction of CO_2 with these ILs is related to the formation of cation- or anion- CO_2 adducts. Here, we show that the use of basic IL that forms buffer-like solutions with DMSO/aqueous media enables the selective catalytic hydrogenation of CO_2 through the naked Ru clusters/NPs, resulting in high efficiency production of the free FA (Scheme 1). In this contribution, surface-cleaned Ru clusters and NPs were prepared by magnetron sputtering into the SILPs. The hydrophilic and hydrophobic nature of the SILPs selectivity not only controlled the growth of the clusters/NPs but also governed the catalytic activity. We showed that the Ru clusters/SILPs displayed higher catalytic activity and selectivity to free FA (not formate salt) as compared to Ru NPs supported on pristine SiO_2 .

2. Experimental

HPLC grade solvents were purchased from Sigma-Aldrich chemicals. The 1-butyl-3-methyl-imidazolium acetate (BMIm.OAc) IL was synthesized as reported elsewhere [38,39]. Hydrogen (> 99.999 %) and carbon dioxide (> 99.999 %) were obtained from Air-liquid Ltd, Brazil. All the NMRs spectra were measured using a Bruker AVANCE III 500 MHz.

2.1. Sputtering depositions of Ru clusters/NPs onto SILPs

In a typical procedure, 2.0 g of SILP was placed in an aluminum conical Al flask inside a deposition chamber. Then, the pressure of the chamber was lowered to 1.6×10^{-6} mbar. Afterward, the pressure was raised to 5.4×10^{-2} mbar with argon at a flow rate of 5 mL/min. The deposition process took place with a power of 100 W, with a current of 225 mA per a time of 43 min. The flask was rotated at a frequency of 18 Hz to maintain continuous homogenization of the supports. After metal deposition, the argon was vented into chamber. The catalysts were

stored under an argon atmosphere for characterization and application.

Note: No free IL (BMIm.OAc) was added in SILP during sputtering deposition.

2.2. Evaluation of Catalytic performance

The catalytic experiments were evaluated in 25 mL Fischer-porter reactor made of stainless steel with a glass lining, stainless steel glass-lined Fischer-porter reactor. Typically, 20 mg of the catalyst was added in the solution of DMSO (2.84 g, 36.4 mmol), H_2O (33 mg, 1.8 mmol) and IL. To eliminate atmospheric impurities, the reactor was flushed with CO_2 . Then the reactor was filled with 32 bar of gas mixture of CO_2 and H_2 (1:2) and the reaction was conducted at desire temperature and time in silicon oil bath. After the reaction, the reactor was cooled in ice-cold water and then cautiously vented. The produced FA was directly analyzed by ^1H NMRs using DMSO-d₆ solvent. TONs were calculated by mole of FA formed per mole of Ru surface atoms [40].

For the recyclability test, the catalyst was isolated through centrifugation, washed twice with 5 mL each of acetone and dichloromethane, and subsequently dried under vacuum at room temperature. Subsequently, the catalyst was added to a fresh IL solution to carry out CO_2 hydrogenation.

3. Results and discussion

3.1. Catalysts preparation and characterizations

Hydrophobic and hydrophilic SILPs supports were prepared by sol-gel process using 1-methyl-3-(3- trimethoxysilylpropyl)-imidazolium cations containing tetrafluoroborate (BF₄⁻) and bis(trifluoromethylsulfonyl)imide (NTf₂⁻) anions (Fig. 1) [41]. The introduction of BF₄⁻ and NTf₂⁻ anions generated the hydrophilic and hydrophobic

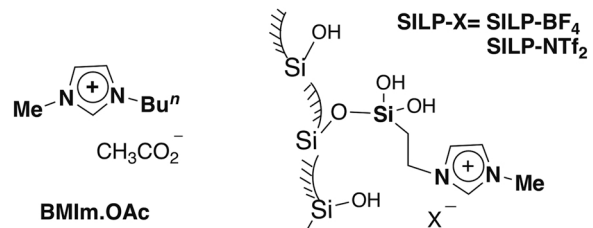
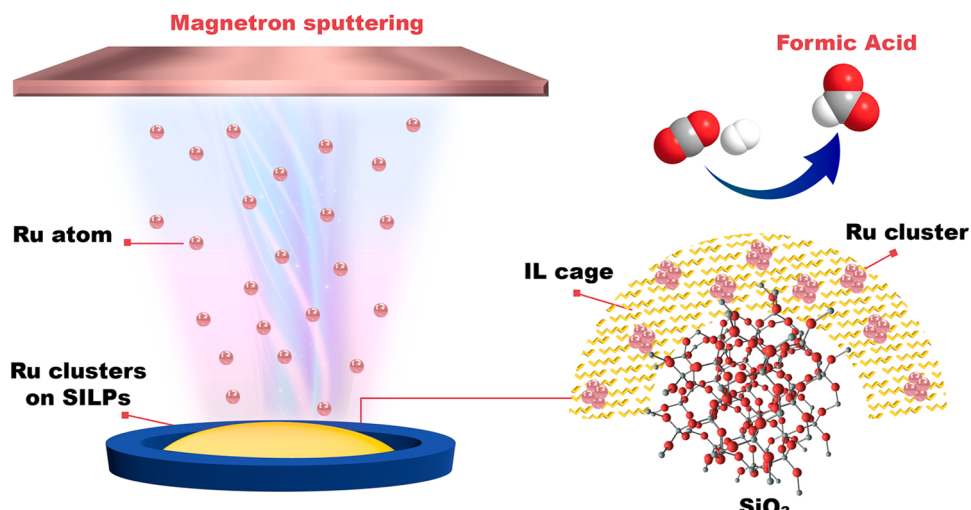


Fig. 1. Structure of SILPs and IL used in this study.



Scheme 1. Schematic representation of the preparation of naked Ru clusters/NPs into SILPs by magnetron sputtering and their CO_2 hydrogenation to “free” formic acid (FA).

properties in SILPs supports, respectively. Solid ^{13}C and ^{29}Si CP-MAS analyses were performed, which confirmed that the ILs were covalently bonded on SiO_2 surface (Fig. S1-S2).

The prepared SILPs was decorated with Ru clusters/NPs by physical deposition employing a “vibrational” sputtering chamber (VSC) that allowed the constant mixing of the solid support during the deposition (Scheme 1) [42]. This method is very simple and allows the generation of “clean” surface MNPs since there are no other chemicals employed in the process [43]. The sputtering deposition of Ru onto SILPs was conducted using 223 mA discharge current to yield clusters and NPs. The presence of the Ru clusters and ultra-small NPs in the supports were confirmed by scanning transmission electron microscopy (STEM) and energy-dispersive X-ray spectroscopy (EDS) of several particles (Figs. 2 and 3).

STEM-HAADF images represented that the visualization of ultra-small Ru NPs on the SILP-BF₄ support is not globally evident, small clusters with the size of 1.02 ± 0.6 nm can be observed (Fig. 2a-b). In the regions where the support was not thick, clusters were detected. The EDS spectrum, even in regions where the Ru clusters were not directly observed, indicates the presence of the Ru element (Fig. 2c-d).

The formation of the Ru clusters and NPs in SILPs may follow the route akin to the thin-film growth on liquids that involves the nucleation, growth of the atomic clusters and aggregation into NPs/branched island [44–46]. ILs can kinetically control the nucleation of the NPs through the interaction between the incoming gaseous atoms and the chemical composition of the ILs [47,48]. The contact ion pair strength (cation-anion interaction) of the ILs can tune the size and shape of the NPs [49,50]. Hence, ILs are adequate media for the stabilization of single atom metal catalysts [51]. Molecular dynamic study showed that Pd clusters with their large induced dipole moments interact strongly with 1,3-dimethylimidazolium tetrafluoroborate (MMIm.BF₄) IL [52]. As a result, BF₄ anion containing IL stabilized the clusters without their further growth to the NPs by providing the high density and a negative charge IL layer. Similar behavior of IL-anion (BF₄) effect is observed in our case where the Ru clusters are formed on SILP having BF₄ anion.

Extremely well distributed small Ru NPs of 1.8 ± 0.3 nm were observed into the SILP-NTf₂ support (Fig. 3a). Whereas, relatively large sized 2.1 ± 0.6 nm Ru NPs in aggregates were revealed into the pristine SiO_2 under similar sputtering conditions (Fig. 3c). Global EDS proved the presence of Ru observed via Z-contrast in HAADF-STEM images (Fig. 3b-c). Of note that the presence of hydrophobic anion in SILP-NTf₂ caused the higher dispersion of Ru NPs. Whereas, agglomeration of Ru NPs was found into SiO_2 where no IL was presented.

Fig. 4a compares the Rutherford backscattering spectrometry (RBS) spectra collected for all samples. The prominent peak observed in the

rising of the Ru *plateau* suggests a higher concentration of Ru on the samples’ surface [53,54]. The surface enrichment with Ru atoms pointed by the RBS results depends on the SILPs properties. Ru/SILP-BF₄ presented sharper peaks as compared to the Ru/SILP-NTf₂ and Ru/ SiO_2 , indicating that BF₄ containing IL favor the anchoring of Ru atoms near to the sample’ surface. Moreover, the sample supported on pure SiO_2 presented the most regular Ru *plateau* indicating a more uniform distribution of Ru atoms on SiO_2 comparing to the samples prepared with IL-modified silica. The compositions of the samples were extracted from RBS (a bulk sensitive technique) data, leading to the Ru concentrations in samples’ bulk presented in Table 1.

The compositions of samples’ surfaces were extracted from the analysis of the X-ray photoelectron spectroscopy (XPS) survey scans (available in Fig. S6). The presence of small amounts of F was observed for all samples except in Ru/ SiO_2 , which represented the presence of IL in SILP-BF₄ and SILP-NTf₂. Fig. 4 also indicates that IL-modified samples also have different concentrations of C on their surfaces. The contributions of ruthenium (Ru 3p_{3/2} peak) and silicon (Si 2p region) were used to estimate the Ru concentration at the samples’ surfaces, which were compared to RBS results as shown in Table 1. The ratio between Ru concentration at the samples’ surface and at samples’ bulk corroborates the qualitative analysis based on RBS data: the use of SILP-BF₄ lead to catalyst with Ru-richer surfaces as compared to the SILP-NTf₂ and, even more, to pristine SiO_2 (Table 1). The chemical environment of Ru atoms at samples’ surfaces was probed by high resolution XPS data collected at Ru 3p and Ru 3d regions. The main results and the parameters extracted from this analysis are available as ESI in Table S1. The Ru 3p doublet (Fig. 4b) was deconvoluted in two chemical components, whose BE and spin-orbit splitting are typical for Ru⁰ (metallic Ru) and Ru⁴⁺ (RuO₂) [55,56]. The Ru⁰ component dominates all samples’ spectra indicating that Ru atoms are mostly in their metallic state in all probed samples’ surfaces. As indicated in Table S1, the contribution of RuO₂ component is slightly higher for sample Ru/SILP-BF₄ (whose Ru atoms are mainly anchored at the surface and therefore more exposed) than for samples Ru/SILP-NTf₂ (in which the Ru distribution is in the depth).

The Ru 3d region has a strong overlap with C 1s region, which hinders the analysis of Ru 3d doublet, due to low Ru amount. Fig. 4c showed the photoemission data collected at Ru 3d + C 1s region for Ru/SILP-BF₄ and Ru/ SiO_2 , whose survey scans’ analysis indicated the higher and lower amounts of Ru at the sample’s surface, respectively. Although the C 1s signal dominates the 277–292 eV region, the structure observed at lower BE (~ 281 eV) in both Fig. 4c indicates the presence of Ru atoms at the surfaces of the all samples [20,57]. Moreover, the different intensity of this structure in each data set corroborates that the Ru amount varies between the samples. The chemical ambient of Ru and C atoms

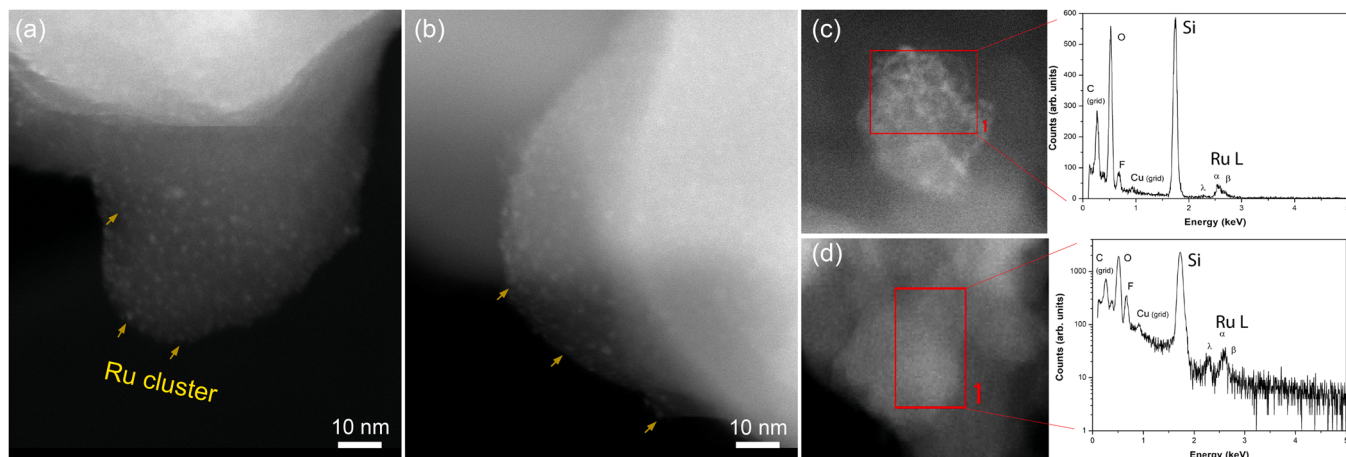


Fig. 2. (a,b) HAADF-STEM images of Ru clusters into SILP-BF₄, (c) HAADF-STEM image and its EDS spectrum at linear scale position and (d) HAADF-STEM image and its EDS spectrum logarithmic scale.

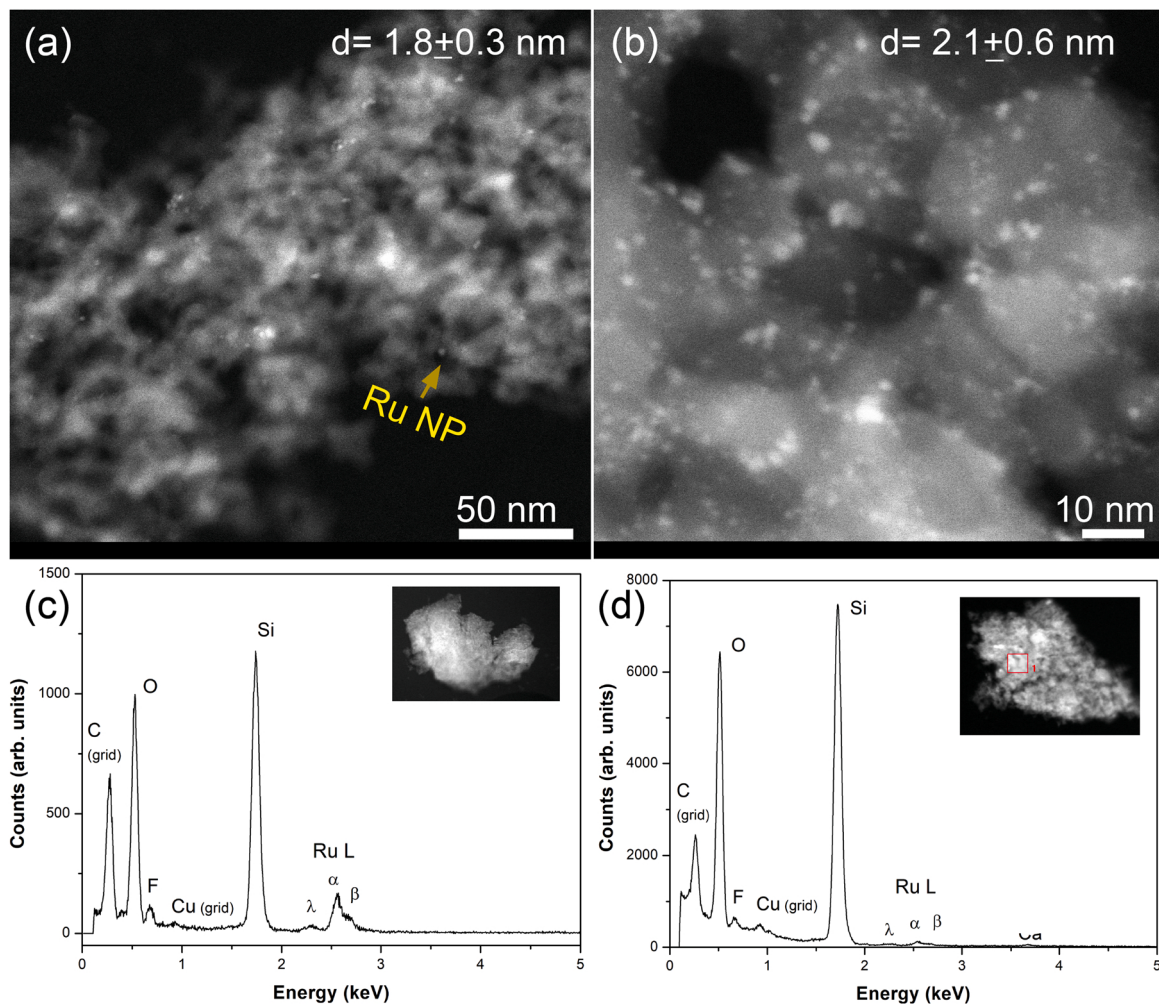


Fig. 3. HAADF-STEM images and EDS spectra of (a,b) Ru NPs into SILP-NTf₂ and (c,d) Ru NPs into pristine SiO₂. (See more images in [supporting information](#)).

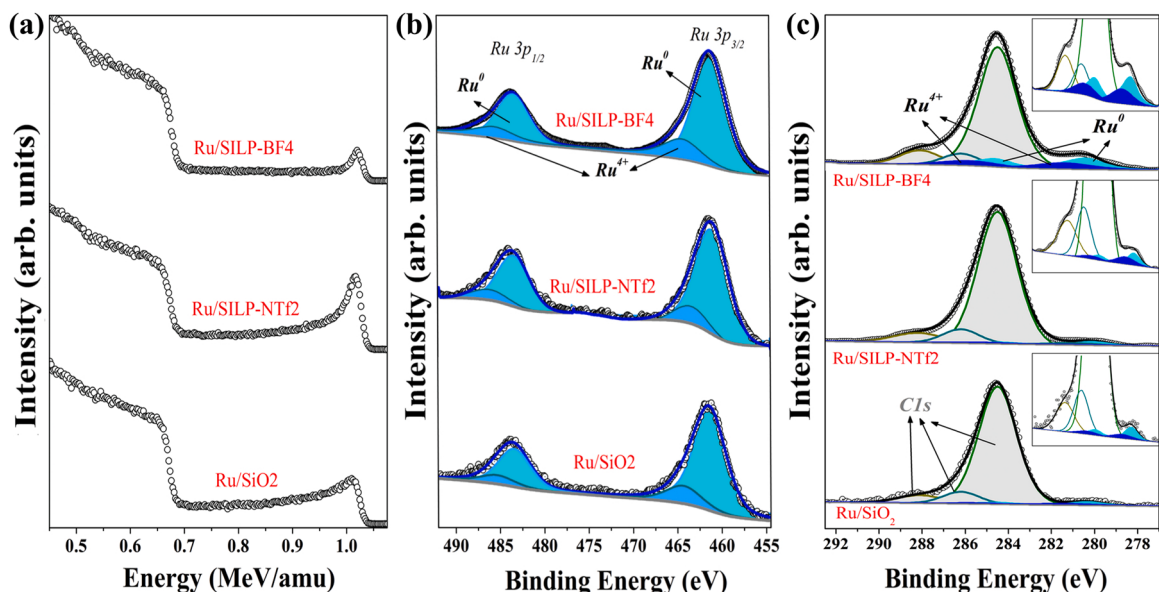


Fig. 4. (a) RBS data collected with 1.2 MeV He⁺ beam incident on Ru-based samples. (b,c) XPS data (open circles), chemical components used in the analysis of Ru 3p and 3d regions (area-filled curves) and the resulting envelopes (blue lines).

Table 1

Ru concentrations obtained by RBS (bulk sensitive) and XPS (surface sensitive).

Catalyst	Ru concentration (wt%) ^a		
	Surface (by XPS)	Bulk (by RBS)	Surface (XPS)/Bulk (RBS) Ratio
Ru/SILP-BF ₄	28	3	9.3
Ru/SILP-NTf ₂	14	7	20
Ru/SiO ₂	12	8	1.5

[a] In the calculation of the Ru loadings in wt% the contributions of F and C were not taken in account.

were investigated through the data deconvolution in five components, whose BEs, FWHMs and relative areas are available in **Table S1**. For Ru 3d doublet, two chemical components (two doublets) were used and assigned to Ru⁰ (280.2 and 284.4 eV) and Ru⁴⁺ (281.5 and 285.8 eV). As well as in Ru 3p region, the metallic component dominates the Ru 3d region and the Ru oxidation is slightly higher for sample Ru/SILP-BF₄. The inset graphs in **Fig. 4c** showed better these components for samples Ru/SILP-BF₄, along with the relative areas of C 1s peak (sum of the three components), Ru⁰ and Ru⁴⁺ (**Table S1**) corroborates the changes in the surface amount of Ru indicated by the survey scan data analysis. Thus, the combined results from RBS and XPS indicated that samples supported on BF₄-modified silica presented higher amounts of Ru at their surfaces as compared to the other samples (**Table 1**). The higher concentration of the surface Ru may be related to the hydrophilic nature and anion population on surface in IL [57]. It has been observed the relative concentration of alkyl chain and BF₄ anion on the IL surface is higher than the alkyl chain and NTf₂ anion [58]. As a result the penetration of Ru atom into the IL-bulk is low in the SILP-BF₄.

3.2. Catalytic performance of CO₂ hydrogenation

The selective CO₂ hydrogenation to FA was evaluated in a batch Fischer-porter reactor using Ru clusters/SILP-BF₄ catalyst in an aqueous solution of 3-n-butyl-1-methylimidazolium acetate (BMIm.OAc) IL at 87 °C under a 32-bar CO₂/H₂ gas mixture (**Table 2**). No FA was observed when the reaction was performed solely in water. Interestingly, 0.12 M of FA was generated with 96 TONs when an aqueous solution of BMIm.OAc IL was used (**Table 2**, entry 1). This efficient activity in aqueous solution of BMIm.OAc IL is attributed to the highly efficiently of the BMIm.OAc IL that absorbs and reacts reversibly with CO₂ to yield bicarbonate (HCO₃⁻) [14]. Moreover, this IL solution can act as IL-water proton buffer solution to stabilise the generated “free” FA during CO₂ hydrogenation. By the introduction of Me-THF and 1,4-dioxane solvents in BMIm.OAc/H₂O, the activity was reached to 120 and 132 TON, respectively (**Table 2**, entries 3–4). On note, almost three-fold (0.50 M) FA was achieved when DMSO was used in combination with BMIm.OAc/H₂O (**Table 2**, entry 5). This dominance of DMSO over other solvents may be because of the intermolecular interactions between IL and DMSO, which lead to loose packing due to the hydrogen bonding of

imidazolium hydrogen atoms with DMSO and shifts the equilibrium to FA [59]. A small amount of H₂O was necessary to accelerate the formation of bicarbonate (HCO₃⁻) and stabilize the formed FA through H-bonding [60].

Since a layer of the imidazolium-based ILs generates ionic-cages around the solid SiO₂ by the combination of their H-bonding and counter-ion pairs. It enriches the local density, tunes the IL orientation close to the surface to facilitate the substantial charge transfer and leading to the reconstruction of the interfacial ionic structure. [61,62] Hence these IL-cages/containers are akin to the membrane in which the geometric and electronic properties of the NPs can be modulated by the proper choice of the IL cations and anions that significantly impacted the diffusion of the reactants, intermediates, and products. [25,28] Of note, the hydrophilic and hydrophobic nature of the SILPs strongly tuned the catalytic activity of the Ru clusters/NPs during the hydrogenation of CO₂ to FA (**Table 3**, **Fig. 5**).

The hydrophilic SILPs (SILP-BF₄) having hydrophilic anions (BF₄⁻) represented remarkable activity (889 TON, 1.13 M FA) as compared to the SILP containing hydrophobic NTf₂ anion (SILP-NTf₂), which showed 779 TON and 0.98 M FA generation (**Table 3**, entries 1–2, **Fig. 5**). This influence can be attributed to hydrophilicity of the BF₄ anion in SILP, which caused the high concentration of the Ru clusters preferentially remained on the surface of the IL (as confirmed by the XPS analysis, **Table 1**). The hydrophilic nature of the support with confine spaces is akin to the catalytic membrane-like device, offering maximum catalytic active sites to activate CO₂ and H₂. The opposite phenomenon was observed in hydrophobic SILPs-NTf₂ in which Ru NPs were penetrated deep into the support, as revealed by the XPS analysis (**Table 1**). This limited the access of CO₂ and H₂, resulting low catalytic activity (**Fig. 5**). It is noteworthy that this IL effect on the catalytic activity was confirmed when pristine Ru/SiO₂ was used in which no IL was presented. The catalytic activity was greatly dropped to 72 TON, resulting in only 0.09 M FA formation (**Table 3**, entry 3). The presence of BF₄ anion induces the hydrophilicity in SILP-BF₄ that keeps the NPs on the surface, while the NTf₂ anion generated the hydrophobicity in SILP-NTf₂ to keep the NPs close to the surface. [41].

CO₂ hydrogenation was also investigated at different temperature from 60° to 120°C by Ru clusters/SILP-BF₄ catalyst (**Fig. 6a**). Interestingly, no FA generation was detected below 65 °C. At 65 °C, a small amount of FA was attained. The FA generation significantly increased with the increased of temperature. When the temperature was reached to 87 °C, about 0.5 M FA was obtained with 396 TONs. While the 0.82 M and 1.2 M FA was achieved at 105 °C and 120 °C, respectively. Of note that no degradation of the BMIm.OAc IL and DMSO was found under our standard conditions at 120 °C, as confirmed by ¹H and ¹³C NMR analyses of the crude reaction (**Fig. S6**). No CO was detected at this temperature (120 °C). An Arrhenius plot was attained on the linear fitting of In TOF versus temperature from 65° to 120°C and resulted an apparent activation energy of 52 ± 3 kJ/mol (**Fig. 6b**). Note that Ea is slightly lower than the activation energies reported for the FA obtained by using Ru-based complexes (58–93 kJ/mol) under similar reaction media. [16, 32] Furthermore, the rate of FA generation was also monitored at

Table 2

Effect of different solvent on CO₂ hydrogenation to formic acid (FA) by Ru clusters/SILP-BF₄ catalyst.^a

Entry	Media	FA [M]	TON
1	H ₂ O	–	–
2	H ₂ O/BMIm.OAc	0.12	96
3	Me-THF/BMIm.OAc/H ₂ O	0.15	120
4	Dioxane/BMIm.OAc/H ₂ O	0.17	132
5	DMSO/BMIm.OAc/H ₂ O	0.50	396
6	DMSO/BMIm.OAc	0.12	96

[a] Reaction conditions: 20 mg Ru/SILP-BF₄ (3 % Ru wt.), 300 mg IL (1.51 mmol), 33 mg H₂O (1.8 mmol), 2.84 g solvent (36.4 mmol), CO₂/H₂ (1:2, 32 bar), 87 °C and 19 h. [b] TON/TOF were calculated on the basis of presence of active atoms of Ru [40].

Table 3

CO₂ hydrogenation to HCO₂H by different catalysts at 87 °C.^a

Entry	Cat.	FA [M]	TON
1	Ru/SILP-BF ₄	1.13	899
2	Ru/SILP-NTf ₂	0.98	779
3	Ru/SiO ₂	0.09	72
4 ^b	Ru/SILP-BF ₄	1.27	4103

[a] Reaction conditions: 20 mg Ru/SILP-BF₄ (3 % Ru wt.), 300 mg IL (1.51 mmol), 33 mg H₂O (1.8 mmol), 2.84 g solvent (36.4 mmol), CO₂/H₂ (1:2, 32 bar) and 64 h. [b] 5.0 mg Ru/SILP-BF₄ (3 % Ru wt.), 400 mg IL (2.02 mmol), 33 mg H₂O (1.8 mmol), 2.84 g DMSO (36.4 mmol), CO₂/H₂ (1:2, 32 bar) and 64 h.

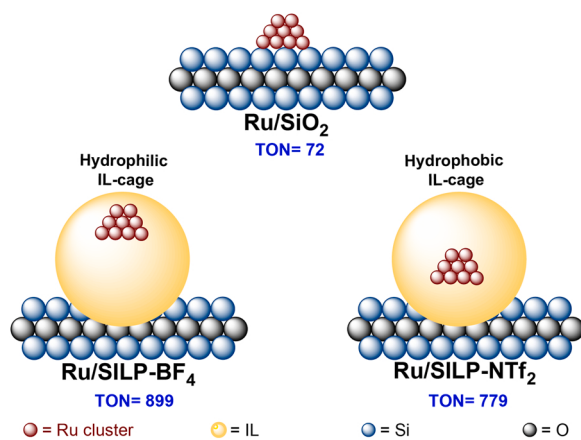


Fig. 5. Graphical representation of the IL-cage effect of hydrophilic (BF₄⁻) and hydrophobic (NTf₂⁻) anions in SILPs having Ru clusters/NPs on the CO₂ hydrogenation to FA.

different reaction time, which augmented linearly with the time (Fig. 6c). At 19 h, 129 TON was obtained that reached to 645 at 36 h with the formation of 0.2 m FA. A significant amount of FA of 0.85 and 1.27 was achieved at 64 and 103 h with 2735 and 4103 TONs, respectively. A total of 2.18 M FA was reached with 7032 TONs. Our catalytic system demonstrated a higher amount of free FA formation and TONs as compared to previously reported heterogeneous catalysts (Table S2, Supporting information).

Moreover, the buffer capacity of the BMIm.OAc IL in our catalytic system was confirmed by obtaining a linear relationship between the FA formed and the amount of the IL (Fig. 6d). The amount of FA increased with the increased of IL amount that provided evidence that IL acted as a buffer. This behavior is consisted by Henderson-Hasselbach equation for buffering systems.[63,64] The IL plays a multiply role; activates the CO₂, stabilize the active intermediates and formed FA as well as stabilize the NPs.

A labelling experiment using ¹³CO₂ was performed to determine the source of carbon in FA generation. ¹³C NMR clearly showed a strong signal at about 166 ppm that was attributed to the H¹³CO₂H (Fig. S8). Whereas, HNMR spectrum of the same solution also represented the formation of H¹³CO₂H from ¹³CO₂ (Fig. S8). Furthermore, Ru clusters/SILP-BF₄ catalyst was recycled five times and showed its stability to the generation of FA (Fig. 7).

3.3. Catalytic CO₂ hydrogenation mechanism

Hydrogenation of CO₂ to FA involved two pathways. One is the direct hydrogenation of CO₂ to FA while the second pathway involves the hydrogenation of CO₂ to formate salts. Until now it has been widely accepted that the mechanism involves the formation of the carbonates which undergo hydrogenation by the metal-hydrides species to generate formate species. While in aqueous solution, HCO₃⁻ are also generated along with the carbonates under basic and/or buffer environment. The hydrogenation of HCO₃⁻ has been ignored. An aqueous solution of the BMIm.OAc IL efficiently absorbs and reacts reversibly with CO₂ yielding HCO₃⁻ [14,65–67]. We propose that the generation of the FA originates

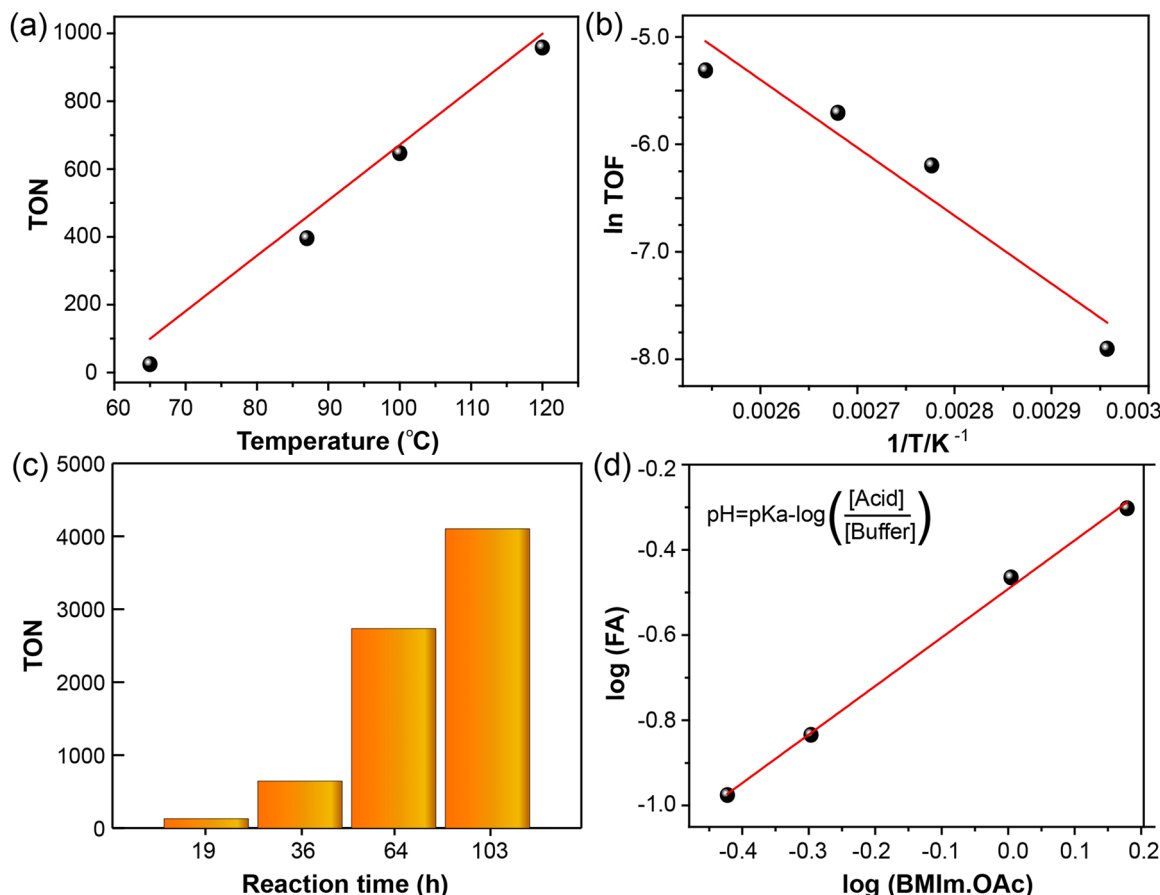


Fig. 6. Effect of temperature of CO₂ hydrogenation to FA (a) and Arrhenius plot (b). Reaction conditions: 20 mg Ru/SILP-BF₄, 300 mg IL (1.51 mmol), 33 mg H₂O (1.8 mmol), 2.84 g solvent (36.4 mmol), CO₂/H₂ (1:2, 32 bar) and 18 h. (c) Time effect vs TON. Reaction conditions: 5 mg Ru/SILP-BF₄, 400 mg IL (2.02 mmol), 33 mg H₂O (1.8 mmol), 2.84 g solvent (36.4 mmol), CO₂/H₂ (1:2, 32 bar) and 87 °C. (d) Relationship between FA and BMIm.OAc IL. Reaction conditions: 20 mg Ru/SILP-BF₄, 2.84 g solvent (36.4 mmol), 33 mg H₂O (1.8 mmol), CO₂/H₂ (1:2, 32 bar), 18 h and 87 °C.

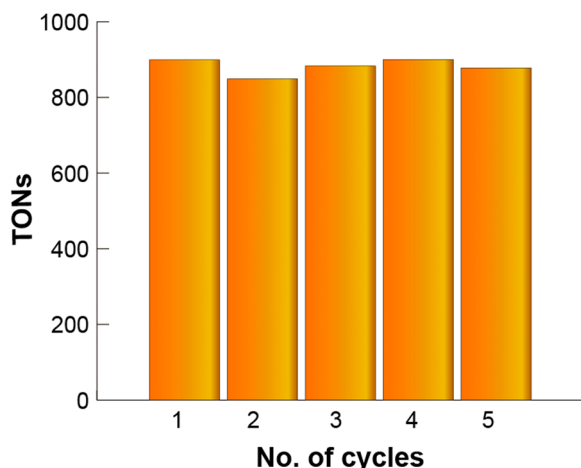


Fig. 7. Reaction conditions: 20 mg Ru/SILP-BF₄, 300 mg IL (1.51 mmol), 33 mg H₂O (1.8 mmol), 2.84 g solvent (36.4 mmol), CO₂/H₂(1:2, 32 bar) and 64 h.

from the hydrogenation of the HCO₃ rather than the direct hydrogenation of the CO₂ in an aqueous solution. For this purpose, DFT calculation was performed to investigate the hydrogenation of HCO₃ to FA on metallic Ru (0001) surface.

To understand the structure-dependent activity of the Ru in the hydrogenation of HCO₃ at atomic level, Density Functional Theory (DFT) calculations were conducted. These calculations were simulated at 298.15 K. A surface geometry of P63/m of Ru 0001 surface was built (Fig. 8A). It has been widely accepted that H₂ undergoes hemolytic

dissociation over the Ru surface and the rate determination of the reaction was the subsequent hydrogenation (Fig. 8A, step c). This is followed by the adsorption of the HCO₃ generated by the BMIm.OAc IL that undergoes hydrogenation to produce formate (HCO₂[−]) as shown in Fig. 8A (Step d). The hydrogenation of the formed HCO₂[−] occurred toward FA.

The calculated energy profile for the hydrogenation of HCO₃ involves eight steps (Fig. 8B). The starting step is the metallic Ru 0001 surface (a). In the following step (b), the H₂ molecule is adsorbed on the surface with adsorption energy of −0.08 eV. The dissociation of the H₂ occurs on Ru with a barrier of −1.37 eV (step-c). Following this, HCO₃ is adsorbed, which undergoes reduction by the attack of hydride with a barrier of −3.61 eV (step-e). This intermediate subsequently generates formate (HCO₂[−]) along with H₂O with the energy barrier of −4.34 eV as shown in step-f. The insertion of H⁺ to the oxygen of HCO₂[−] generated FA with an energy reaction of over −3.70 eV.

4. Conclusions

SILPs were decorated with naked Ru clusters and NPs by the magnetron sputtering. The presence of IL anions (BF₄ and NTf₂) in SILPs kinetically controlled the growth of incoming sputter Ru atoms into clusters and/or nanoparticles. SILPs containing hydrophilic anion (BF₄) facilitated the formation of Ru clusters, while SILPs with hydrophobic anion (NTf₂) resulted in the formation of highly dispersed ultra-small (1.8 ± 0.3 nm) NPs. Moreover, the IL in SILPs generated the confined spaces akin to the solvent-cages that effectively controlled the selective CO₂ hydrogenation to base-free FA. The presence of the hydrophilic anion (BF₄) in SILP promoted a higher population of the Ru clusters on the support surface, providing maximum catalytic active sites for the

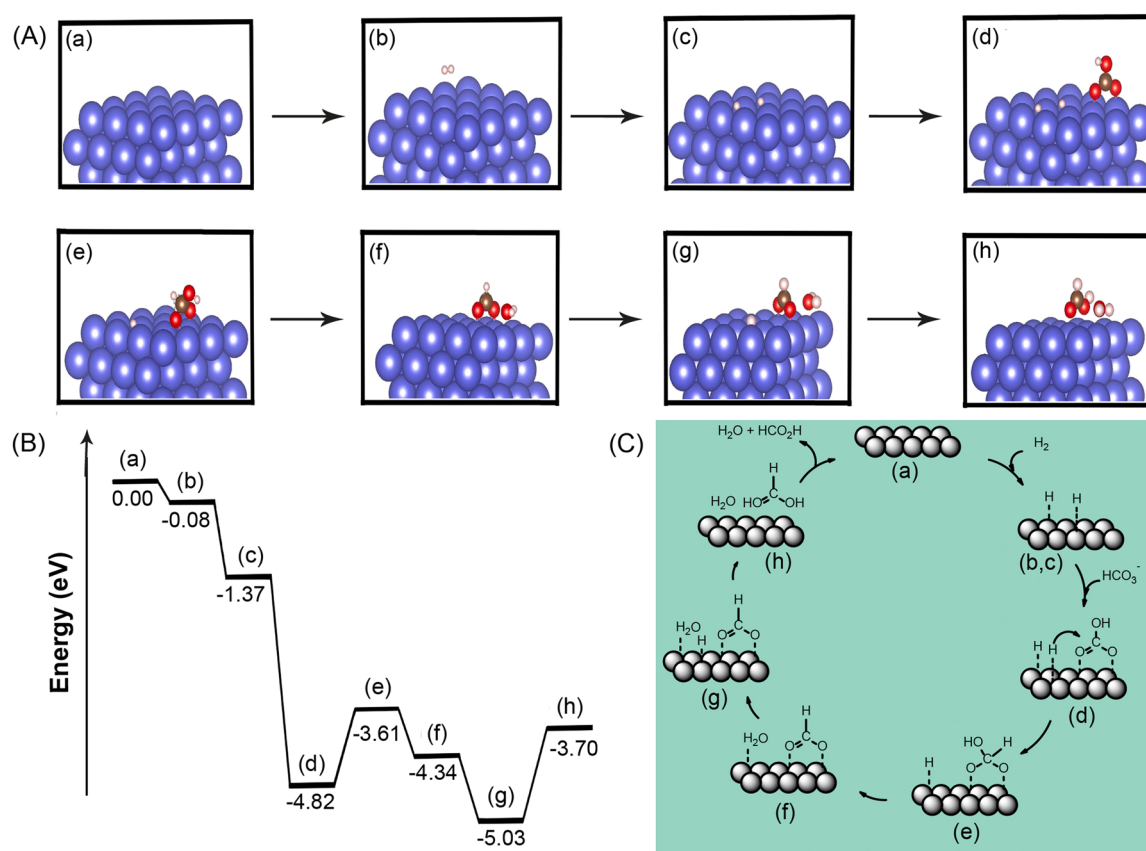


Fig. 8. (A) Ball-and-stick illustrations of the atomic structures: (a) Top and side views of the clean Ru surface, (b) H₂ near (0001) surface, (c) displaying binding of H₂ on (0001) surface, (d) cleavage of H₂ to H⁺ atoms, (e) H⁺ insertion to carbon of HCO₃^{*}, (f) the formation of HCO₂^{*} and H₂O^{*} and (e) H⁺ insertion to O of HCO₂^{*} to form HCO₂H. (B) DFT-calculated adsorption energy, in eV. (C) A reaction pathway for the hydrogenation of HCO₃ to FA on Ru (0001).

activation of the CO₂ and H₂ to FA that led to a significant enhancement in FA generation. The opposite phenomenon was observed in SILPs with hydrophobic NTf₂ anion in which Ru NPs were migrated deep into the support, thereby providing relatively limited access to CO₂ and H₂. As prepared Ru clusters/SILP catalyst showed the remarkable generation of the FA with a yield of 2.2 M and 7305 TONs in BMIm.OAc/DMSO/H₂O media at 87 °C. The mechanism was confirmed by DFT calculations that followed the reaction pathway of the hydrogenation of HCO₃⁺ to the FA.

Associated content

None.

Supporting Information

Experimental details about the ¹³C and ²⁹Si CP-MAS analyses and TGA analyses of the SILPs. HAADF-STEM and XPS analyses of Ru/SILPs and Ru/SiO₂.

CRediT authorship contribution statement

All the authors contributed equally.

Declaration of Competing Interest

The authors declare that they have no known competing financial interests or personal relationships that could have appeared to influence the work reported in this paper.

Data Availability

Data will be made available on request.

Acknowledgment

We are grateful to CAPES (001), FAPERGS (22/2551-0000386-9 and 18/2551-0000561-4) and CNPq (406260/2018-4) for financial support. J.D. is a fellow of the “Maria Zambrano program” at the University of Murcia (Spain). R.B.P. acknowledges CNPq (grant 309599/2021-0) for financial support as well as LaMCAD-UFG, CENAPAD-SP and Cluster Euler/CeMEAI for providing the computational resources. MVC thanks to CAPES (22/2551-0000544-6). DE is grateful to Bluenano for providing Sputtering facility.

Appendix A. Supporting information

Supplementary data associated with this article can be found in the online version at [doi:10.1016/j.apcatb.2023.123315](https://doi.org/10.1016/j.apcatb.2023.123315).

References

- P. Markewitz, W. Kuckshinrichs, W. Leitner, J. Linssen, P. Zapp, R. Bongartz, A. Schreiber, T.E. Müller, Worldwide innovations in the development of carbon capture technologies and the utilization of CO₂, *Energy Environ. Sci.* 5 (2012) 7281–7305, <https://doi.org/10.1039/c2ee03403d>.
- J.G. Canadell, C. Le Quéré, M.R. Raupach, C.B. Field, E.T. Buitenhuis, P. Ciais, T. J. Conway, N.P. Gillett, R.A. Houghton, G. Marland, Contributions to accelerating atmospheric CO₂ growth from economic activity, carbon intensity, and efficiency of natural sinks, *Proc. Natl. Acad. Sci. USA* 104 (2007) 18866–18870, <https://doi.org/10.1073/pnas.0702737104>.
- F. Raganati, F. Miccio, P. Ammendola, Adsorption of carbon dioxide for post-combustion capture: a review, *Energy Fuels* 35 (2021) 12845–12868, <https://doi.org/10.1021/acs.energyfuels.1c01618>.
- O.V. Ogidiama, T. Shamim, Assessment of CO₂ capture technologies for CO₂ utilization in enhanced oil recovery, *Greenh. Gases: Sci. Technol.* 11 (2021) 432–444, <https://doi.org/10.1002/ghg.2057>.
- J. Artz, T.E. Müller, K. Thenert, J. Kleinekorte, R. Meys, A. Sternberg, A. Bardow, W. Leitner, Sustainable conversion of carbon dioxide: an integrated review of catalysis and life cycle assessment, *Chem. Rev.* 118 (2018) 434–504, <https://doi.org/10.1021/acs.chemrev.7b00435>.
- J. Dupont, Across the Board: Jairton Dupont, *Chemsuschem* 8 (2015) 586–587, <https://doi.org/10.1002/cssc.201403276>.
- V.K. Tomazett, G. Chacon, G. Marin, M.V. Castegnaro, R.P. das Chagas, L.M. Lião, J. Dupont, M.I. Qadir, Ionic liquid confined spaces controlled catalytic CO₂ cycloaddition of epoxides in BMIm.ZnCl₃ and its supported ionic liquid phases, *J. CO₂ Util.* 69 (2023), 102400, <https://doi.org/10.1016/j.jcou.2023.102400>.
- P.K. Sahoo, Y. Zhang, S. Das, CO₂-promoted reactions: an emerging concept for the synthesis of fine chemicals and pharmaceuticals, *ACS Catal.* 11 (2021) 3414–3442, <https://doi.org/10.1021/acscatal.0c05681>.
- R. Cauwenbergh, S. Das, Photochemical reduction of carbon dioxide to formic acid, *Green Chem.* 23 (2021) 2553–2574, <https://doi.org/10.1039/D0GC04040A>.
- Y. Zhang, T. Zhang, S. Das, Catalytic transformation of CO₂ into C1 chemicals using hydrosilanes as a reducing agent, *Green Chem.* 22 (2020) 1800–1820, <https://doi.org/10.1039/C9GC04342J>.
- R. Cauwenbergh, V. Goyal, R. Maiti, K. Natte, S. Das, Challenges and recent advancements in the transformation of CO₂ into carboxylic acids: straightforward assembly with homogeneous 3d metals, *Chem. Soc. Rev.* 51 (2022) 9371–9423, <https://doi.org/10.1039/D1CS00921D>.
- S. Enthaler, J. von Langermann, T. Schmidt, Carbon dioxide and formic acid—the couple for environmental-friendly hydrogen storage? *Energy Environ. Sci.* 3 (2010) 1207–1217, <https://doi.org/10.1039/B907569k>.
- M. Ali, A. Gual, G. Ebeling, J. Dupont, Ruthenium-catalyzed hydroformylation of alkenes by using carbon dioxide as the carbon monoxide source in the presence of ionic liquids, *Chemcatchem* 6 (2014) 2224–2228, <https://doi.org/10.1002/cetc.20140226>.
- N.M. Simon, M. Zanatta, F.P. dos Santos, M.C. Corvo, E.J. Cabrita, J. Dupont, Carbon dioxide capture by aqueous ionic liquid solutions, *ChemSusChem* 10 (2017) 4927–4933, <https://doi.org/10.1002/cssc.201701044>.
- T. Yasuda, E. Uchigae, T. Fujitani, K.-i Tominaga, M. Nishida, Reverse water gas shift reaction using supported ionic liquid phase catalysts, *Appl. Catal. B: Environ.* 232 (2018) 299–305, <https://doi.org/10.1016/j.apcatb.2018.03.057>.
- A. Weilhard, M.I. Qadir, V. Sans, J. Dupont, Selective CO₂ hydrogenation to formic acid with multifunctional ionic liquids, *ACS Catal.* 8 (2018) 1628–1634, <https://doi.org/10.1021/acscatal.7b03931>.
- C.I. Melo, A. Szczepanska, E. Bogel-Lukasik, M. Nunes da Ponte, L.C. Branco, Hydrogenation of carbon dioxide to methane by ruthenium nanoparticles in ionic liquid, *ChemSusChem* 9 (2016) 1081–1084, <https://doi.org/10.1002/cssc.201600203>.
- Z. Zhang, Y. Xie, W. Li, S. Hu, J. Song, T. Jiang, B. Han, Hydrogenation of carbon dioxide is promoted by a task-specific ionic liquid, *Angew. Chem.* 120 (2008) 1143–1145, <https://doi.org/10.1002/ange.200704487>.
- M.I. Qadir, J. Dupont, Thermo- and photocatalytic activation of CO₂ in ionic liquids nano-domains, *Angew. Chem. Int. Ed.*, N./a (2023), e202301497, <https://doi.org/10.1002/anie.202301497>.
- M.I. Qadir, F. Bernardi, J.D. Scholten, D.L. Baptista, J. Dupont, Synergistic CO₂ hydrogenation over bimetallic Ru/Ni nanoparticles in ionic liquids, *Appl. Catal. B: Environ.* 252 (2019) 10–17, <https://doi.org/10.1016/j.apcatb.2019.04.005>.
- S.J. Louis Anandaraj, L. Kang, S. DeBeer, A. Bordet, W. Leitner, Catalytic hydrogenation of CO₂ to formate using ruthenium nanoparticles immobilized on supported ionic liquid phases, *Small*, N./a (2023), 2206806, <https://doi.org/10.1002/smll.202206806>.
- C. Sievers, O. Jimenez, T.E. Müller, S. Steuernagel, J.A. Lercher, Formation of solvent cages around organometallic complexes in thin films of supported ionic liquid, *J. Am. Chem. Soc.* 128 (2006) 13990–13991, <https://doi.org/10.1021/ja064204c>.
- M. Sobota, M. Happel, M. Amende, N. Paape, P. Wasserscheid, M. Laurin, J. Libuda, Ligand Effects in SCILL model systems: site-Specific Interactions with Pt and Pd nanoparticles, *Adv. Mater.* 23 (2011) 2617–2621, <https://doi.org/10.1002/adma.201004064>.
- M. Sobota, M. Schmid, M. Happel, M. Amende, F. Maier, H.P. Steinruck, N. Paape, P. Wasserscheid, M. Laurin, J.M. Gottfried, J. Libuda, Ionic liquid based model catalysis: interaction of BMIM Tf2N with Pd nanoparticles supported on an ordered alumina film, *Phys. Chem. Chem. Phys.* 12 (2010) 10610–10621, <https://doi.org/10.1039/c003753b>.
- L. Luza, C.P. Rambor, A. Gual, F. Bernardi, J.B. Domingos, T. Grehl, P. Brüner, J. Dupont, Catalytically active membranelike devices: ionic liquid hybrid organosilicas decorated with palladium nanoparticles, *ACS Catal.* 6 (2016) 6478–6486, <https://doi.org/10.1021/acscatal.6b01813>.
- A. Weilhard, G. Abarca, J. Viscardi, M.H.G. Precht, J.D. Scholten, F. Bernardi, D. L. Baptista, J. Dupont, Challenging thermodynamics: hydrogenation of benzene to 1,3-cyclohexadiene by Ru@Pt nanoparticles, *Chemcatchem* 9 (2017) 204–211, <https://doi.org/10.1002/cetc.201601196>.
- P. Migowski, P. Lozano, J. Dupont, Imidazolium based ionic liquid-phase green catalytic reactions, *Green Chem.* 25 (2023) 1237–1260, <https://doi.org/10.1039/D2GC04749G>.
- L. Luza, C.P. Rambor, A. Gual, J. Alves Fernandes, D. Eberhardt, J. Dupont, Revealing hydrogenation reaction pathways on naked gold nanoparticles, *ACS Catal.* 7 (2017) 2791–2799, <https://doi.org/10.1021/acscatal.7b00391>.
- S. Wesselbaum, U. Hintermair, W. Leitner, Continuous-flow hydrogenation of carbon dioxide to pure formic acid using an integrated scCO₂ process with immobilized catalyst and base, *Angew. Chem. Int. Ed.* 51 (2012) 8585–8588, <https://doi.org/10.1002/anie.201203185>.
- D. Wei, H. Junge, M. Beller, An amino acid based system for CO₂ capture and catalytic utilization to produce formates, *Chem. Sci.* 12 (2021) 6020–6024, <https://doi.org/10.1039/D1SC00467K>.

[31] A. Moazezbarabadi, D. Wei, H. Junge, M. Beller, Improved CO₂ capture and catalytic hydrogenation using amino acid based ionic liquids, *ChemSusChem* 15 (2022), e202201502, <https://doi.org/10.1002/cssc.202201502>.

[32] A. Weilhard, S.P. Argent, V. Sans, Efficient carbon dioxide hydrogenation to formic acid with buffering ionic liquids, *Nat. Commun.* 12 (2021), 231, <https://doi.org/10.1038/s41467-020-20291-0>.

[33] A. Weilhard, K. Salzmann, M. Navarro, J. Dupont, M. Albrecht, V. Sans, Catalyst design for highly efficient carbon dioxide hydrogenation to formic acid under buffering conditions, *J. Catal.* 385 (2020) 1–9, <https://doi.org/10.1016/j.jcat.2020.02.027>.

[34] L. Piccirilli, B. Rabell, R. Padilla, A. Riisager, S. Das, M. Nielsen, Versatile CO₂ hydrogenation-dehydrogenation catalysis with a Ru-PNP/ionic liquid system, *J. Am. Chem. Soc.* 145 (2023) 5655–5663, <https://doi.org/10.1021/jacs.2c10399>.

[35] P.R. Upadhyay, V. Srivastava, Selective hydrogenation of CO₂ gas to formic acid over nanostructured Ru-TiO₂ catalysts, *RSC Adv.* 6 (2016) 42297–42306, <https://doi.org/10.1039/c6ra03660k>.

[36] V. Srivastava, Functionalized hydrotalcite tethered ruthenium catalyst for carbon sequestration reaction, *Catal. Lett.* 148 (2018) 1879–1892, <https://doi.org/10.1007/s10562-018-2399-z>.

[37] P.R. Upadhyay, V. Srivastava, Ionic liquid mediated in situ synthesis of Ru nanoparticles for CO₂ hydrogenation reaction, *Catal. Lett.* 147 (2017) 1051–1060, <https://doi.org/10.1007/s10562-017-1995-7>.

[38] C.C. Cassol, G. Ebeling, B. Ferrera, J. Dupont, A simple and practical method for the preparation and purity determination of halide-free imidazolium ionic liquids, *Adv. Synth. Catal.* 348 (2006) 243–248, <https://doi.org/10.1002/adsc.200505295>.

[39] J. Qiu, Y. Zhao, Z. Li, H. Wang, M. Fan, J. Wang, Efficient ionic-liquid-promoted chemical fixation of CO₂ into α -alkylidene cyclic carbonates, *ChemSusChem* 10 (2017) 1120–1127, <https://doi.org/10.1002/cssc.201601129>.

[40] A.P. Umpierre, E. dejesús, J. Dupont, Turnover numbers and soluble metal nanoparticles, *ChemCatChem* 3 (2011) 1413–1418, <https://doi.org/10.1002/cctc.201100159>.

[41] L. Luza, A. Gual, C.P. Rambor, D. Eberhardt, S.R. Teixeira, F. Bernardi, D. L. Baptista, J. Dupont, Hydrophobic effects on supported ionic liquid phase Pd nanoparticle hydrogenation catalysts, *Phys. Chem. Chem. Phys.* 16 (2014) 18088–18091.

[42] R. Bussamra, D. Eberhardt, A.F. Feil, P. Migowski, H. Wender, D.P. de Moraes, G. Machado, R.M. Papaleo, S.R. Teixeira, J. Dupont, Sputtering deposition of magnetic Ni nanoparticles directly onto an enzyme surface: a novel method to obtain a magnetic biocatalyst, *Chem. Commun.* 49 (2013) 1273, doi:papers2://publication/doi/10.1039/c2cc38737a.

[43] H. Wender, P. Migowski, A.F. Feil, S.R. Teixeira, J. Dupont, Sputtering deposition of nanoparticles onto liquid substrates: recent advances and future trends, *Coord. Chem. Rev.* 257 (2013) 2468–2483, <https://doi.org/10.1016/j.ccr.2013.01.013>.

[44] S.-J. Yu, Y.-J. Zhang, J.-X. Chen, H.-L. Ge, Growth mechanism of iron films on silicone oil surfaces prepared by sputtering method, *Surf. Rev. Lett.* 13 (2006) 779–784, <https://doi.org/10.1142/s0218625x06008840>.

[45] Y.-J. Zhang, S.-J. Yu, Experimental observations of disk-shaped patterns In Fe films sputtering deposited on silicone oil surfaces, *Int. J. Mod. Phys. B* 23 (2009) 3147–3157, <https://doi.org/10.1142/s0217979209049772>.

[46] S.-J. Yu, Y.-J. Zhang, Formation mechanism and surface evolution of silver films sputtering deposited on silicone oil substrates, *Surf. Rev. Lett.* 15 (2008) 525–530, <https://doi.org/10.1142/s0218625x0801172x>.

[47] M.I. Qadir, A. Kauling, G. Ebeling, M. Fartmann, T. Grehl, J. Dupont, Functionalized ionic liquids sputter decorated with Pd nanoparticles, *Aust. J. Chem.* 72 (2019) 49–54.

[48] M.I. Qadir, A. Kauling, L. Calabria, T. Grehl, J. Dupont, Fabrication of naked silver nanoparticles in functionalized ionic liquids, *Nano-Struct. Nano-Objects* 14 (2018) 92–97, <https://doi.org/10.1016/j.nanoso.2018.01.015>.

[49] J. Adamski, M.I. Qadir, J.P. Serna, F. Bernardi, D.L. Baptista, B.R. Salles, M. A. Novak, G. Machado, J. Dupont, Core-Shell Fe-Pt nanoparticles in ionic liquids: magnetic and catalytic properties, *J. Phys. Chem. C* 122 (2018) 4641–4650, <https://doi.org/10.1021/acs.jpcc.7b12219>.

[50] J. Dupont, From molten salts to ionic liquids: a "nano" journey, *Acc. Chem. Res.* 44 (2011) 1223–1231, <https://doi.org/10.1021/ar2000937>.

[51] S. Ding, Y. Guo, M.J. Hulse, B. Zhang, H. Asakura, L. Liu, Y. Han, M. Gao, J.-y Hasegawa, B. Qiao, T. Zhang, N. Yan, Electrostatic stabilization of single-atom catalysts by ionic liquids, *Chem* 5 (2019) 3207–3219, <https://doi.org/10.1016/j.chempr.2019.10.007>.

[52] E.E. Zvereva, S.A. Katsyuba, P.J. Dyson, A.V. Aleksandrov, Solvation of palladium clusters in an ionic liquid: a QM/MM molecular dynamics study, *J. Phys. Chem. C.* 120 (2016) 4596–4604, <https://doi.org/10.1021/acs.jpcc.5b11229>.

[53] L. Bruno, M. Urso, Y. Shacham-Diamand, F. Priolo, S. Mirabella, Role of substrate in Au nanoparticle decoration by electroless deposition, *Nanomaterials* 10 (2020) 2180.

[54] M.I. Qadir, M. Zanatta, J. Pinto, I. Vicente, A. Gual, E.F. Smith, B.A.D. Neto, P.E. N. de Souza, S. Khan, J. Dupont, J. Alves Fernandes, Reverse semi-combustion driven by titanium dioxide-ionic liquid hybrid photocatalyst, *ChemSusChem* 13 (2020) 5580–5585, <https://doi.org/10.1002/cssc.202001717>.

[55] D.J. Morgan, Resolving ruthenium: XPS studies of common ruthenium materials, *Surf. Interface Anal.* 47 (2015) 1072–1079, <https://doi.org/10.1002/sia.5852>.

[56] J. Wang, C. Yuan, N. Yao, X. Li, Effect of the nanostructure and the surface composition of bimetallic Ni-Ru nanoparticles on the performance of CO methanation, *Appl. Surf. Sci.* 441 (2018) 816–823, <https://doi.org/10.1016/j.apsusc.2018.02.070>.

[57] M.I. Qadir, M.V. Castegnaro, F.F. Selau, M. Samperi, J.A. Fernandes, J. Morais, J. Dupont, Catalytic semi-water–gas shift reaction: a simple green path to formic acid fuel, *ChemSusChem* 13 (2020) 1817–1824, <https://doi.org/10.1002/cssc.201903417>.

[58] C. Kolbeck, T. Cremer, K.R.J. Lovelock, N. Paape, P.S. Schulz, P. Wasserscheid, F. Maier, H.P. Steinrück, Influence of different anions on the surface composition of ionic liquids studied using ARXPS, *J. Phys. Chem. B* 113 (2009) 8682–8688, <https://doi.org/10.1021/jp902978r>.

[59] B.A. Marekha, K. Sonoda, T. Uchida, T. Tokuda, A. Idrissi, T. Takamuku, ATR-IR spectroscopic observation on intermolecular interactions in mixtures of imidazolium-based ionic liquids CnmimTFSA (n=2–12) with DMSO, *J. Mol. Liq.* 232 (2017) 431–439, <https://doi.org/10.1016/j.molliq.2017.02.068>.

[60] K. Rohmann, J. Kothe, M.W. Haenel, U. Englert, M. Hölscher, W. Leitner, Hydrogenation of CO₂ to formic acid with a highly active ruthenium acriphos complex in DMSO and DMSO/Water, *Angew. Chem. Int. Ed.* 55 (2016) 8966–8969, <https://doi.org/10.1002/anie.201603878>.

[61] R.M. Lynden-Bell, M.G. Del Pópolo, T.G.A. Youngs, J. Kohanoff, C.G. Hanke, J. B. Harper, C.C. Pinilla, Simulations of ionic liquids, solutions, and surfaces, *Acc. Chem. Res.* 40 (2007) 1138–1145, <https://doi.org/10.1021/ar700065s>.

[62] Y. Wang, H. He, C. Wang, Y. Lu, K. Dong, F. Huo, S. Zhang, Insights into ionic liquids: from Z-bonds to quasi-liquids, *JACS Au* 2 (2022) 543–561, <https://doi.org/10.1021/jacsau.1c00538>.

[63] H.N. Po, N.M. Senozan, The Henderson-Hasselbalch equation: its history and limitations, *J. Chem. Educ.* 78 (2001) 1499, <https://doi.org/10.1021/ed078p1499>.

[64] R. de Levie, The Henderson approximation and the mass action law of Guldberg and Waage, *Chem. Educ.* 7 (2002) 132–135, <https://doi.org/10.1007/s00897020562a>.

[65] S.J. Cobb, V.M. Badiani, A.M. Dharani, A. Wagner, S. Zacarias, A.R. Oliveira, I.A. C. Pereira, E. Reisner, Fast CO₂ hydration kinetics impair heterogeneous but improve enzymatic CO₂ reduction catalysis, *Nat. Chem.* 14 (2022) 417–424, <https://doi.org/10.1038/s41557-021-00880-2>.

[66] M. Zanatta, N.M. Simon, J. Dupont, The nature of carbon dioxide in bare ionic liquids, *ChemSusChem* 13 (2020) 3101–3109, <https://doi.org/10.1002/cssc.202000574>.

[67] M.I. Qadir, A. Weilhard, J.A. Fernandes, I. de Pedro, B.J.C. Vieira, J. C. Waerenborgh, J. Dupont, Selective carbon dioxide hydrogenation driven by ferromagnetic RuFe nanoparticles in ionic liquids, *ACS Catal.* 8 (2018) 1621–1627, <https://doi.org/10.1021/acscatal.7b03804>.